Gemini Surfactant Abetted Synthesis Of Mesoporous Mn/Mg Bimetal Doped TiO_2 Nanomaterial: Characterization And Photocatalytic Activity Studies Under Visible Light Irradiation

Sankara Rao Miditana
Andhra University
Siva Rao Tirukkovalluri (sivaraoau@gmail.com)
Andhra University https://orcid.org/0000-0001-5156-1885
Imandi Manga Raju
Andhra University
Shaik Abdul Alim
Andhra University
Genji Jaishree
Andhra University
M.L.V. Prasanna Chippada
Andhra University

Research

Keywords: Mn2+/Mg2+ bimetal doped TiO2, Gemini Surfactant, Mehtyl Red, Mesoporous Nanocatalyst, Sol-gel technique, Anatase TiO2

Posted Date: July 28th, 2020

DOI: https://doi.org/10.21203/rs.3.rs-45648/v1

Version of Record: A version of this preprint was published at Sustainable Environment Research on February 10th, 2021. See the published version at https://doi.org/10.1186/s42834-021-00078-8.

Abstract

The present work mainly aimed to synthesize different weight percentages (0.25 Wt% - 1.00 Wt%) of Manganese (Mn^{2+}) and Magnesium (Mg^{2+}) bimetal ions doped TiO_2 nanomarerial assisted with different weight percentages (5 Wt% - 15 Wt%) of Gemini Surfactant (GS) using sol-gel method. The bimetal doped and undoped TiO_2 photocatalysts were characterized by XRD, SEM, EDX, FT-IR, UV Vis-DRS, TEM, BET and PL. Characterization results evinced that Mn^{2+}/Mg^{2+} bimetal ions doping and encapsulation of GS on TiO_2 nanoparticles promote the formation of mesoporous multi-particle anatase TiO_2 nanocatalysts with narrowed band gap, less particle size and high surface area. The surface elemental composition of the MMT5-GS2 (after calcination) revealed the presence of both the metal dopants Mn^{2+} and Mg^{2+} along with the Ti and O and their chemical interactions were further confirmed by FT-IR results. The photocatalytic activity of these catalysts was assessed by the degradation of Methyl Red (MR) using visible light irradiation. To understand the effect of different reaction parameters on the photocatalytic activity of the nanocatalysts such as the dopant concentration, GS concentration, catalyst dosage, solution pH and initial dye concentrations were investigated and optimized to achieve best performance. The photoluminescence results conclude that OH radicals are the crucial reactive species responsible for oxidative photocatalytic degradation of MR.

1. Introduction

It is worth to note that among the different semiconductors that are being studied from past few decades for the photocatalytic degradation of various organic pollutants from wastewater, TiO_2 stands as the most preferable one due to its non-toxicity, non-corrosive, photo stability and low cost. To make it suitable for visible light activity, many attempts are being made to modify the TiO_2 electronic structure to overcome its disadvantages of high band gap energy and high rate of electron-hole recombination. The recent literature findings revealed that bimetal ions doping into TiO_2 crystal lattice had overcome the above drawbacks and significantly enhanced its visible light activity [1–3]. Among the various metal ion dopants studied so far, transition metal ion dopants can greatly reduce the bad gap and electron-hole recombination by forming an extra energy level below the conduction band of TiO_2 due to interaction of their 3d or 4d states with Ti 3d states [4]. Recently, K.V. Divya laksmi et al. reported that Manganese is most preferable among the transition metals owing to the presence of t_2g orbital of d is very close to conduction band of TiO_2 by which the absorption can be possibly shifted to visible part of the spectrum [5]. On the other hand, Changneng Zhang et al., Desta shumuye et al. and Sofiaou et al. were investigated the effect of Magnesium, an alkaline earth metal on the crystalline structure and catalytic activity of TiO_2 and found its absorption band was shifted more towards visible region, which resulted in performing high photocatalytic activity [6–8]. Hence, Mn^{2+} and Mg^{2+} ions could be more effective as metal ion dopants to modify the TiO_2 for better photocatalytic performance under visible light irradiation.

As the size, shape and surface area of the photocatalyst plays major role in photocatalytic degradation process of organic pollutants from wastewater, surfactants were the best reported species to control the growth and agglomeration of nanoparticles during the synthesis process. Among those surfactants, more surface-active anionic Gemini surfactant, 1,4-Butane sultone is the most suitable as a capping agent to fabricate the spherical shaped bimetal doped TiO_2 nanoparticles with small grain size and large surface area [9]. Hence, in the present study we aimed to synthesize the Mn^{2+} and Mg^{2+} bimetal doped TiO_2 naoparticles in the presence of Gemini surfactant using sol-gel process through which we can achieve high purity and homogeneous materials at room temperatures under stoichiometry control [10].

Compared to bulk materials nanomaterials possesses unique physical, chemical and mechanical properties. To understand overall properties, it is important to characterize the structural, optical and morphological properties of nanomaterials prior to proceed for different applications to obtain better results [11]. Hence, several advanced sophisticated techniques were used in the present study to characterize the crystalline phase, surface morphology, elemental composition, visible light absorption capacity, particle size and surface area of as synthesized bimetal doped TiO_2 nanoparticles to understand its suitability for potocatalytic degradation applications.

Due to the widespread industrial activities, various organic dye pollutants are being discharged into water bodies causing severe water pollution. Almost, 15% of the dyes produced worldwide are lost during synthesis and processing with wastewater. Moreover, 50% of all the dyes used in various industries are carcinogenic azo dyes, which are characterized by one or more azo bonds (-N = N -) [12] among which, Methyl Red is a familiar azo dye and is widely used in paper printing, textile dyeing and leather industries [13]. It causes skin & eye irritation and irritation of respiratory & digestive tract and is a suspected carcinogen, mutagen and mitotic poison [14].

Hence, removal of these pollutants from waste waters in an eco-friendly way is stands as a present major research concern. Therefore, in the present study, we attempted to remove this model azo dye pollutant from the contaminated water using as synthesized Mn^{2+}/Mg^{2+} bimetal doped TiO_2 nanocatalysts and their photocatalytic efficiency was tested by optimizing the important reaction parameters like dopant concentration, surfactant concentration, pH, catalyst dosage and initial concentration of the dye for the better water pollution abatement.

2. Experimental

2.1. Materials

All the chemicals used in this research were of reagent grade and used without any further purification. Titanium tetra-n-butoxide (Ti(OBu)4), Manganese nitrate $[Mn(NO_3)_2].6H_2O$ and Magnesium Nitrate $[Mg(NO_3)_2].6H_2O$ purchased from E-Merck Germany were used as precursors of TiO_2, Mn and Mg respectively, for preparing Mn^{2+}/Mg^{2+} bimetal doped TiO_2 samples. For the surfactant assisted bimetal doped TiO_2 catalysts, 1,4-butane sultone obtained from Sigma Aldrich (Germany) was used. Methyl red

(High media, India.) was used as a model azo dye pollutant for photocatalytic degradation studies. Milli-Q water used for the preparation of all the solutions.

2.2. Synthesis of nanocatalyst

Manganese and Magnesium bimetal ions doped nanotitania and gemini surfactant assisted Mn^{2+}/Mg+2+ bimetal doped TiO_2 samples were prepared by sol-gel method. In this method, titanium tetra-n-butoxide (10 mL) was added to ethanol (20 mL) and acidified with 1.4 mL of HNO_3 taken in a pyrex glass vessel (Solution-I) and stirred for 20 min. Desired wt% (0.25 wt% - 1.0 wt%) of Mn^{2+} and Mg^{2+} dopants proportionate to TiO_2 weight were taken in ethanol (20 mL) in another beaker and added 4.5 mL of Milli-Q water for effective hydrolysis purpose (Solution-II). Then the solution-II was slowly added to solution-I dropwise with continuous stirring. A colloidal solution that formed after complete mixing is further stirred for 90 min and aged for 48 h to obtain the gel. The formed gel was dried (at 70 ^oC), ground and calcined at 450 ^oC for about 5 h in a furnace. To get homogeneous powder the calcined samples were well ground after cooling.

To optimize the best dopant concentrations, the photocatalytic efficiency of the as synthesized bimetal doped TiO_2 samples were tested by degrading Methyl red dye and 0.25 wt% Mn^{2+} and 1.00 wt% Mg^{2+} doped TiO_2 (MMT5) was found to be the best. For further enhancement in the photocatalytic activity of the MMT5 catalyst, Gemini surfactant assisted MMT5 nanocatalysts were synthesized by following the same procedure but different wt% (5 wt%, 10 wt% and 15 wt%) of Gemini surfactant was added after the mixing of solution-I and solution-II. To study and compare the effect of dopants and surfactant on the photocatalytic properties of bimetal doped TiO_2, undoped TiO_2 sample was prepared using the same procedure without adding dopants and surfactant precursors. Details of all the synthesized catalysts are presented in Table.1.

2.3. Characterization techniques

The crystalline structure of photocatalysts were studied by powder X-ray diffraction (XRD) spectra using PANanalyticaldifractometer with CuKα radiation (λ=0.15405 nm) operated at 45 kV, 40 mA and 0.2 scan rate. Based on the Scherrer equation using full width at half maximum (FWHM), crystallite size of TiO_2 nanocatalysts was determined. The Diffuse reflectance spectra (DRS) of the catalysts were recorded in the range of 200-800 nm with a Shimadzu 3600 UV-Visible-DRS Spectrophotometer using $BaSO_4$ as reference. Scanning electron microscopy (SEM, JSM 6300, Japan) equipped with energy dispersive X-Ray (EDX) spectroscopy was used to investigate the surface morphology and elemental analysis, respectively. The microstructure and particle size of the samples were analysed by high resolution transmission electron microscopy (HRTEM) JEM-2100 JEOL at an operating voltage of 200 kV. Fourier transform infrared spectra (FT-IR) of the nanocatalysts were recorded on a FT-IR spectrometer (Nicolet Avatar360). Brunauer- Emmet-Teller (BET) surface area, pore size and pore volume of the nanocatalysts were determined using Quanta Chrome Nova 2200E system by recording N_2 adsorption-desorption isotherms

at 77.3 k. Photoluminescence (PL) analysis was performed by Hitchi F-7000 fluorescence spectrophotometer. The pH of the reaction mixture and the amount of MR degraded during the photocatalytic process were adjusted and monitored using Elico Digital pH meter (Model IIIE, EI) and UV–vis spectrophotometer (Shimadzu 1601), respectively.

2.4. Experimental procedure for determination of visible light photocatalytic activity of nanocatalyst

The photocatalytic activity of surfactant assisted Mn^{2+}/Mg^{2+} bimetal ions doped TiO_2 nanocatlyst was examined by the degradation of a model azo dye pollutant, Methyl Red in a previously reported visible light photoreactor [15]. For visible light illumination, high-pressure metal halide lamp (400 W, 35,000 lm, 436-546 nm output) has been used and placed 20 cm away from the pyrex glass vessel containing 100 mL of MR dye solution of desired concentration (1–10 mgL^{-1}) with sufficient amount of the catalyst. To screen IR effect and to keep constant temperature (25 °C) during the degradation experiments, water was passed continuously around the reaction vessel. Prior to visible light irradiation, the pH of the reaction mixture was adjusted to desired value by addition of 0.1 N NaOH/0.1 N HCl and the reaction mixture was stirred in dark for 30 min to establish the adsorption-desorption equilibrium between MR dye and surface of the catalyst [16]. After the visible light irradiation, 5 mL aliquots of samples were collected at regular time intervals using Millipore syringe (0.45 µm) and change in the concentration of MR dye during the degradation process was studied with a UV–vis spectrophotometer (Shimadzu 1601) by measuring its absorbance at 525 nm. The percentage degradation of MR was determined by using the following equation [17].

$$\%\ \text{degradation of MR} = \frac{C_0 - C_t}{C_0} \times 100$$

Where, C_0 is the initial concentration of MR dye solution before degradation and C_t is the concentration at time t. For the better photocatalytic degradation, the effect of reaction parameters like concentration of dopants, surfactant concentration, pH of the solution, catalyst dosage and initial dye concentration was studied and optimized by varying the measured parameter while keeping other parameters constant and the results are discussed in section 4.1-4.5. As the photocatalytic degradation of organic pollutants is mainly initiated by highly oxidative OH radicals, which can be easily captured by fluorescent probe molecules, the formation of •OH in the photocatalysis process was studied by photoluminescence (PL) technique using coumarin as a probe molecule [17].

3. Results And Discussion

3.1. X-ray Diffraction Study

From the XRD patterns of all the synthesized catalysts shown in Fig.1 (a) & (b), all samples including undoped TiO_2 calcined at 450 ºC for 5 h showed the formation of anatase phase having characteristic high intensity diffraction peak at 2θ = 25.3º along with other corresponding small diffraction peaks at 2θ

values 37.9º, 48.05º and 54.1º that can be indexed to planes of (101), (004), (200) and (211) of anatase phase respectively (JCPDS No. 21-1272). No extra peak found at 2θ=27.8º, indicated that there is no formation of rutile phase. As the ionic radii of Mn^{2+} (0.78Å) and Mg^{2+} (0.72Å) are closer to the ionic radii of Ti^{4+} (0.68 Å), Mn^{2+} and Mg^{2+} dopant metal ions were expected to substitute Ti^{4+} ions in TiO_2 matrix which is confirmed by the absence of any diffraction peaks related to Mn and Mg oxides or other compounds [18,19]. And it is also known that as the Mn^{2+} and Mg^{2+} are more electro positive, the electronic cloud in each TiO_2 might be loosely held, favoring the formation of less dense anatase phase [20]. The average crystallite sizes of the undoped, bimetal-doped (MMT) and surfactant assisted co-doped (MMT-GS) catalysts were calculated based on the full width at half maximum (FWHM) of the characteristic high intensified peak using Scherrer equation [1] ($d = k\lambda / \beta \cos\theta$), where d is the average crystallite size, k is 0.9 (Scherrer constant), λ is 1.5406 Å (X-ray wavelength), β is the full width at half maximum (FWHM) and θ is the diffraction angle and are tabulated in Table 2. From the table, the average crystallite size of the catalysts found to be ranging from 7.21-10.22 nm, 10.86-12.87 nm and 18.30 nm for surfactant assisted co-doped (MMT-GS), bimetal doped (MMT) and undoped TiO_2 nanocatalysts respectively. The substitutional doping of metal ions into the TiO_2 lattice inhibited the grain growth by formation of Ti–O–Mn and Ti-O-Mg due to which the crystallite size was decreased in MMT catalysts. Further decrease in crystallite size was observed for the catalyst prepared in presence of surfactant (MMT-GS), which can be attributed to the effective capping nature of the Gemini surfactant which controls the nucleation and minimizes the agglomeration of TiO_2 nanoparticles during synthesis process [21].

3.2. UV-Visible Diffuse Reflectance Spectra Study (UV–vis. DRS)

From the UV-visible diffuse reflectance spectra of the undoped TiO_2, bimetal doped TiO_2 (MMT) and surfactant assisted co-doped TiO_2 (MMT-GS) nanomaterials shown in Fig. 2 (a), it is observed that absorbance bands are shifted more towards the higher wavelengths i.e. red shifted in MMT and MMT-GS catalysts compared to undoped TiO_2, which is possible due to the decreased band gap by co-doping of Mn^{2+} and Mg^{2+} into the TiO_2 matrix. The decrease in band gap can be ascribed to the joint effect of these two metal dopant ions (Mn^{2+} & Mg^{2+}) in MMT and MMT-GS system, where these formed the extra energy levels below the conduction band of TiO_2 and thus reduces the electron-hole recombination by trapping electrons and enhances the visible light absorbance. From the Fig. 2(b) it is further confirmed by band gap energies obtained for all the synthesized catalysts using Kubelka-Monk formalism and Tauc plot method [22]. The corresponding band gap energy values are presented in Table 2. From the table, it is found that the average band gap values of the photocatalysts are in the range of 2.66-2.83 eV, 2.68-2.97 eV and 3.20 eV for surfactant bimetal doped (MMT-GS), bimetal doped (MMT) and undoped TiO_2, respectively. These outcomes revealed that all MMT and MMT-GS catalysts are visible light active and can be used as better photocatalysts. The catalysts MMT5, MMT5-GS1, MMT5-GS2 and MMT5-GS3 have same weight percentage of Mn and Mg; consequently, they have the absorption peaks nearly at the

same wavelength. But in particular, among all the MMT's and GS assisted bimetal doped catalysts, MMT5-GS2 showed least band gap energy i.e. 2.66 eV.

Before proceeds to the further characterization we have conducted trial photocatalytic degradation experiments for all the synthesized catalysts using MR dye. From the results it was noticed that among all the bimetal doped TiO_2 catalysts, 0.25 wt% Mn^{2+}& 1.00 wt% Mg^{2+} bimetal doped TiO_2 (MMT5) exhibited better photocatalytic activity and moreover MMT5 assisted with 10 wt% of GS (MMT-GS2) has shown some more enhanced photocatalytic activity. Hence, we selected these two particular catalysts for further characterization with SEM-EDX, TEM, BET, FT-IR and photoluminescence study.

3.3. Scanning Electron Microscopy and Energy Dispersive X- ray Spectroscopy (SEM-EDX)

The FESEM images shown in Fig. 3 (a), (b) and (c) illustrates the surface morphology of undoped TiO_2, MMT5 and MMT5-GS2, respectively. On comparison, it can be clearly seen that the morphology of the TiO_2 has been changed from large aggregates with scratchy surface in undoped TiO_2 (Fig.3(a)) to multiparticle agglomerated irregular shaped particles with rough surface in MMT5 and pseudospherical less agglomerated nanoparticles with smooth surface area and less particle size in MMT-GS2. This is clearly indicating that Mg^{2+} and Mn^{2+} bimetal ions doping and capping action with Gemini surfactant have a significant impact on the morphology of TiO_2 nanoparticles which controlled the grain growth and particle nucleation.

In addition, chemical composition of MMT-GS2 sample was investigated by EDX and the results are depicted in the Fig. 4. Along with the Ti and O elements of TiO_2, the dopant elements Mn and Mg are found in the spectra supports the presence of dopants in the TiO_2 matrix and there is no GS associated peaks are found in the spectra indicated complete elimination of GS after the calcination process. The quantitative analysis results are listed in a table inserted in Fig.4 describes weight percentage as well as atomic percentage of the compositional elements of the sample which indicates good compatibility with the dopant concentration used for the synthesis of TiO_2 nanoparticles.

3.4. Transmission Electron Microscope (TEM)

The TEM images of MMT5 and MMT5-GS2 photocatalysts are shown in Fig.5 (a) and (b) respectively. The TEM image (Fig.5 (a)) of bimetal doped TiO_2 (MMT-5) shows pseudospherical shaped with multiparticle agglomeration and an average particle size of 6.6 nm. Where as in MMT5-GS2 (Fig.5 (b)), most of TiO_2 particles are well dispersed with very low agglomeration compare to Fig. 5 (a) and the particle size is in the range of 2.3-5.4 nm, with an average particle size of 3.8 nm. Thus, it clearly indicates that the Gemini surfactant was effectively inhibited the particle overgrowth and aggregation and resulted in less particle size with increased surface area, which is well correlated with BET results given in Table.2. The selected area electron diffraction (SAED) patterns shown in Fig. 5(c) confirmed the anatase phase with good crystallinity indexed by the concentric rings, which is in good agreement with XRD diffraction patterns. In addition to SAED, from the HR-TEM image of MMT5-GS2 (Fig.5(d)) the observed lattice

fringes with d-spacing of 0.352 nm are corresponds to (101) plane of anatase and further confirms the single crystal nature and high crystallinity of anatase TiO_2 [23].

3.5. Fourier Transform Infrared Spectroscopy (FT-IR)

The incorporation of metal ion dopants, Mn^{2+} and Mg^{2+} into TiO_2 lattice was further confirmed by FT-IR results. The FT-IR spectra of the undoped TiO_2, MMT5 and MMT5-GS2 (before and after calcination) were shown in Fig. 6 (a-d). The peaks at 3403.01 cm^{-1}, 2926.10 cm^{-1}, 1616.36 cm^{-1}, 1383.78 cm^{-1}, 3378.14 cm^{-1}, 2918.69 cm^{-1}, 1626.67 cm^{-1} and 1372.07 cm^{-1} are corresponds to stretching vibrations of surface O-H and 3351.79 cm^{-1}, 2918.72 cm^{-1}, 1619.40 cm^{-1} and 1383.80 cm^{-1} corresponds to the and bending vibrations of adsorbed H_2O molecules [24]. The stretching vibrations of Ti-O and bending vibrations of Ti-O-Ti observed at 575.41 cm^{-1} and 1375.78 cm^{-1} in undoped TiO_2 (Fig.6a) were deformed/shifted to 620.32 cm^{-1} and 1300.12 cm^{-1} in MMT5 (Fig.6b) and 540.01 cm^{-1} and 1182.01 cm^{-1} in MMT5-GS2 (Fig.6c & d) respectively, which can be attributed to the presence of dopants in TiO_2 lattice. Hence, FT-IR study confirms that Mn^{2+} and Mg^{2+} are substitutionally doped into TiO_2 lattice by replacing Ti^{4+} and formed new network i.e Ti-O-Mn and Ti-O-Mg which are in good agreement with the previous reports [25,26]. The FT-IR spectra of 1,4- butane sultone (GS) is shown in Fig.S1 as a supplementary file. The bands situated at about 2945.62 cm^{-1}, 1447.80 cm^{-1}, 1345.72 cm^{-1}, 1246.03 cm^{-1}, 1149.79 cm^{-1}, 1059.62 cm^{-1} and 996.59 cm^{-1} in GS were shifted to 2855.77 cm^{-1}, 1734.95 cm^{-1}, 1459.87 cm^{-1}, 1206.73 cm^{-1}, 1136.50 cm^{-1}, 1094.06 cm^{-1} and 982.86 cm^{-1} in MMT5-GS2 before calcinations (BC) shown in Fig.6(c) which confirms the existence of strong electrostatic interaction between GS and surface of catalyst in MMT5-GS2 before calcinations [27].

From Fig. 6d, absence of these peaks confirms that there was no surfactant remained in the synthesized catalyst, MMT5-GS2 after calcinations (AC). This indicated that due to calcination at 450 °C, surfactant is completely eliminated from nanocatalyst.

3.6. Brunauer-Emmett-Teller (BET) surface area analysis

To study the effect of bimetal doping and GS on the surface area and porosity nature of the as synthesized TiO_2 nanoparticles of undoped TiO_2, MMT5 and MMT5-GS2N_2, N_2 adsorption- desorption isotherms and their corresponding Berret- Johner- Halenda (BJH) pore size distribution plots were recorded and presented in Fig.7(a-b). From Fig.7(a), it results a type -IV isotherm with H_2 hysteresis loop, characteristic of the ordered mesoporous structure of the catalyst [28]. The average surface area, A_{BET} (m^2/g) of all prepared catalysts was determined and tabulated in Table.2.

From the Table 2 the bimetal doped TiO_2 (MMT) has shown increased surface area (112.03 m^2/g) compared to undoped TiO_2 (64.09 m^2/g) due to crystal growth suppression by dopants. Whereas catalyst prepared in presence of GS surfactant (MMT5-GS2) shows higher surface area (230.20 m^2/g) compared to both MMT5 and undoped TiO_2. It could be the strong evident for the decreased particle size of the TiO_2

resulted from effective capping ability of the surfactant, which restricts the particle growth and nucleation during the synthesis process. To better compare the effect of bimetal doping and capping of GS on as synthesized TiO_2 nanoparticles over single Mn^{2+} and Mg^{2+} doped TiO_2, comparative results are tabulated by referencing Mn and Mg single doped literature repots in table 3.

3.7. Photoluminescence Spectra (PL)

One of the essential reactive species in the process of photocatalysis is hydroxyl radical (•OH) and is responsible for oxidation reactions. Because of high reactivity and short life of hydroxyl radical, it is impossible for direct detection. To inspect the production of hydroxyl radicals from the catalyst during the photocatalysis reaction, photoluminescence technique has been adopted using coumarin as a fluorescent probe molecule, which on reaction with hydroxyl radicals yields the 7-hydroxy coumarin [17]. In this technique, 0.10 g of catalyst is dispersed in 100 mL of 10 ppm coumarin solution in acidic conditions and illuminated to visible light irradiation. Small aliquots of reaction solution samples were withdrawn for every 30 min, filtered and photoluminescence intensity was measured in the range of 350-600 nm with excitation fixed at a wavelength of 435 nm. It has been observed from Fig.8 that in between of 440-460 nm there exist photoluminescence spectra of the generated 7-hydroxy coumarine with maximum emission at 450 nm. A linear increase in photoluminescence intensity was observed with increasing irradiation time. However, in the absence of irradiation no excitation was observed for the sample (0 min in Fig.8).

From the above results, it could be understood that the number of hydroxyl radicals produced on the catalyst surface was directly proportional to the irradiation time. The results further assure that the synthesized nanomaterial showed the enhanced rate of formation of hydroxyl radicals under irradiation to visible light. This is due to the fact that the already formed photo holes in the valence band of bimetal doped TiO_2 could directly react with H_2O/OH^- to produce hydroxyl radical [31].

4. Evaluation Of Photocatalytic Activity Of Synthesized Mmt-gs Nanocatalysts By Degradation Of Methyl Red

Visible light assisted catalytic activity of the synthesized MMT-GS photocatalysts were evaluated by degradation of MR. For the better photocatalytic degradation, the effect of reaction parameters like concentration of dopants, surfactant (GS) concentration, pH of the solution, catalyst dosage and initial dye concentration was studied and optimized as follows.

4.1. Effect of Metal ion dopant (Mn^{2+} & Mg^{2+}) Concentration

In order to find out and optimize the best dopant concentration of bimetal doped photocatalyst among all the synthesized MMT photocatalysts, degradation experiments were carried out with each photocatalyst under visible light irradiation by taking catalyst dosage 0.05 g, pH-4 and initial MR concentration 10 mg/L. The rate of degradation of MR has been studied by measuring the MR absorbance, which is

inserted in Fig. 9. It can be seen from the figure that photocatalytic performance was found better for all the bimetal doped TiO_2 photocatalysts than undoped one and in specific among all the synthesized photocatalysts, the best catalytic performance was shown by 0.25 wt% of Mn^{2+} & 1.00 wt% of Mg^{2+} bimetal doped TiO_2 (MMT5). This can be attributed to its narrowed band gap resulted from the impurity energy levels between the valence band and conduction band that were created by the presence of both metal dopants which helps in the generation of more electron-hole pairs. And also, its less crystallite size and high surface area facilitates the adsorption of a greater number of dye molecules on its surface for the degradation [7]. Therefore, based on the above results MMT5 was selected for the optimizing other parameters.

4.2. Effect of Gemini surfactant concentration

To find out the optimal concentration of GS in MMT5 photocatalyst for efficient photocatalytic performance, as synthesized MMT5-GS catalysts with various wt% of GS (5 wt%, 10 wt% and 15 wt%) along with MMT5 were tested by degradation of MR under visible light irradiation by maintaining other parameters constant i.e. catalyst dosage is 0.05 g, pH 4 and initial MR concentration 10 mgL^{-1}. It is observed from the Fig.10 that all MMT5 nanocatalysts prepared in presence of GS degraded the MR in less time compared to MMT5 (Fig.9) which clearly indicated the significant role of the capping nature of the GS on the photocatalytic activity of MMT catalysts. From the apparent rate constants obtained by slopes of the individual curves (insect of Fig.10) it can be clearly seen that the degradation rate was increased up to 10wt% GS concentration (MMT5-GS2) and then decreased on further loading. It could be due to the fact that increased GS concentration may restrict the effective doping of the metal ions into TiO_2 crystal lattice. Hence, MMT5-GS2 i.e.0.25 wt % Mn^{2+} & 1.00 wt % Mg^{2+} at 10 wt% of Gemini surfactant had been taken as a catalyst for further studies.

4.3. Effect of pH

According to Tang et al., [32] for charged substrates like TiO_2, there is a significant dependency on the pH value for the effective photocatalytic degradation, because the overall surface charge and adsorptive properties of TiO_2 nanomaterial depend strongly on solution pH. Hence, in this study the effect of pH on the catalytic performance of the MMT5-GS2 was carried out by ranging the pH from 2 to 8 and keeping other parameters constant i.e. catalyst dosage 0.1 g and initial dye concentration 10 mgL^{-1}. From Fig.11 it was observed that the degradation of MR is high in acidic medium compared to basic medium. This may be due to the strong electrostatic interaction between positively charged surface (H^+ ions) of the catalyst and negatively charged dye molecules. When the pH increased to basic medium the catalyst surface acquires negative charge and electro statically repels the like charged dye molecules. In specific, the degradation of MR was high at pH 4, because positive charge (H^+ ions) on TiO_2 surface increases and negatively charged MR can easily adsorbed on the surface of catalyst. And further increase in pH greater than 4 will facilitate the hydrolysis of metal ions on the surface of TiO_2 which seize its photocatalytic activity.

4.4. Effect of Catalyst dosage:

To avoid the wastage of catalyst and minimize screening effect, a number of experiments were carried out to get the optimum photocatalyst dosage by varying its amount ranging from 0.025 to 0.1 g using 10 mgL^{-1} of 100 mL of MR solution at pH 4. It was observed from Fig.12 that the degradation of the dye increased linearly with increase of catalyst loading up to 0.05 g because of the increased total surface area for dye adsorption. But after increasing the photocatalyst beyond 0.05 g, it creates turbidity and agglomeration of the catalyst particles due to excess photocatalyst and reduces the light transmission through the solution which leads to less photocatalytic activity [33]. And also, collisions between active molecules and ground state molecules of bimetal doped TiO_2 results in deactivation of the catalyst particles [17].

4.5. Effect of initial concentration of dye

To study the effect of initial concentration of dye (MR) at a fixed weight of catalyst (0.05 g) and pH4, the experiments were carried out with different concentrations of MR dye from 5 mg/L to 15 mg/L and results are presented in Fig.13. The results demonstrate that the rate of degradation of MR dye increased up to 10 mg/L. But, further increase in dye concentration causes deactivation of the catalyst due to the blanket effect [34]. And because of fixed catalyst dosage (0.05g) there is no possibility to produce sufficient number of OH radicles to counteract the increased number of dye molecules. Hence, the rate of degradation decreases.

5. Conclusions

Gemini surfactant abetted mesoporous Mn^{2+}/Mg^{2+} bimetal doped TiO_2 nanocatalysts were successfully synthesized by sol-gel method without change in the crystallinity of TiO_2 nanoparticles. The effective charge separation and narrowed band gap created by Mn^{2+}/Mg^{2+} bimetal ions doping and reduced particle size and increased surface area resulted from capping of GS had significantly enhanced the photocatalytic performance of MMT5-GS2 nanocatalyst towards the degradation of MR dye under visible light irradiation. The photoluminescence results exhibited that OH radicals are the crucial reactive species responsible for oxidative photocatalytic degradation of MR. The highest degradation of MR was achieved in 60 min at optimized reaction conditions of 10 wt% GS on 0.25 wt% Mn^{2+} / 1.00 wt% Mg^{2+} bimetal ions doped TiO_2, solution pH 4, catalyst loading of 0.05 g and initial MR concentration 10 mg/L. Based on its effective photocatalytic activity, MMT5-GS2 nanocatalyst could be used as a promising material for abatement of water pollution caused by organic dyes.

Abbreviations

XRD: X-ray Diffraction, SEM: Scanning Electron Microscopy, EDX: Energy Dispersive X-ray Spectroscopy, FT-IR: Fourier Transform Infrared Spectroscopy, UV Vis-DRS: UV-Visible Diffused Reflectance

Spectroscopy, TEM: Transmission Electron Microscopy, BET: Brunauer-Emmett-Teller surface area analyzer, PL: Photoluminescence Spectroscopy.

Declarations

Availability of data and materials:

All data generated or analysed during this study are included in this published article [and its supplementary information files].

Competing interests: The authors declare that they have no competing interests

Funding: Not Applicable

Authors' contributions:

SRM: Conceptualization; Data curation; Formal analysis; Investigation, Methodology; Software; Writing original draft.

TSR: Supervision; Conceptualization; Methodology; Resources; Writing Original draft

IMR: Data curation; Formal Analysis; Software; Writing original draft; Review & editing.

SAA, GJ and MLVPC: Methodology; Formal Analysis; Data curation.

Acknowledgements: Not Applicable

References

1. Wang, C. Chen, F. Wu, B. Zou, M. Zhao, J. Wang, C. Feng, J. Hazard. Mater. 164, 615-620 (2019).
2. Malika, Ch.V. Rao, R.K. Das, A.S. Giri, A.K Golder, Appl. Surf. Sci. 368, 316–324 (2016).
3. R. Chelli, A.K. Golder, European Water 58, 53-60 (2017).
4. Wang, R. Zhang, J. Li, L. Li, S. Lin, Nanoscale Res. Lett. 9:46 (2014).
5. V.D. Lakshmi, T.S. Rao, J.S.P, I.M. Raju, S.K.A. Alim, P. Kalyani, Environ. Nanotech. Monitor. & Manage. 10, 494–504 (2018).
6. Zhang, S. Chen, L. Mo, Y. Huang, H. Tian, L. Hu, Z. Huo, S. Dai, F. Kong, X. Pan, J. Phys. Chem. C, 115, 16418-16424 (2011).
7. S. Meshesha, R.C. Matangi, S.R. Tirukkovalluri, S. Bojja, J. Asian Ceram. Soc. 5, 136–143 (2017).
8. V. Sofianou, M. Tassi, N. Boukos, S. Thanos, T. Vaimakis, J. Yu, C. Trapalis, Catal. Today, 230, 125–130 (2014).
9. D. Chekuri, S.R. Tirukkovalluri, South Afric. J. Chem. Eng. 24, 183-195 (2017).
10. G. Akpan, B.H. Hameed, Appl. Catal. A: Gen. 375 (1), 1–11 (2010).

11. J. Ikhmayies, JOM 66, 28-29 (2014).
12. L. Buitron, M. Quezada, G. Moreno, Bioresour. Technol. 92, 143-149 (2004).
13. Lachheb, E. Puzenat, A. Houas, M. Ksibi, E. Elaloui, C. Guillard, J.M. Herrmann, Appl. Catal. B: Environ. 39, 75-90 (2002).
14. Sahoo, A.K. Gupta, A. Pal, Desalination 181, 91-100 (2005).
15. C.S. Wu, C.H. Chen, J. Photochem. Photobiol. A: Chem. 163, 509–515 (2004).
16. V.D. Lakshmi, T.S. Rao, J.S. Padmaja, I.M. Raju, M.R. Kumar, Chin. J. Chem. Eng. 27, 1630–1641 (2019).
17. M. Raju, T.S. Rao, K.V.D. Lakshmi, M.R. Chandra, J.S. Padmaja, G. Divya, J. Environ. Chem. Eng. 7, 103211 (2019).
18. D. Shannon, Acta Cryst. A 32, 751-767 (1976).
19. Venkatachalam, M. Palanichamy, V. Murugesan, J. Molec. Catal. A: chem. 273, 177-185 (2007).
20. D. Jeong, Pramod H. Borse, J.S. Jang, J.S. Lee, Ok-S. Jung, H. Chang, J.S. Jin, M.S. Won, H.G. Kim, J. Cera. Proces. Res. 9(3), 250-253 (2008).
21. S. Padmaja, T.S. Rao, K.V.D. Lakshmi, I.M. Raju, J. Environ. Chem. Eng. 6, 6457-6467 (2018).
22. Ghobadi, Int. Nano Lett. 3, 2 (2013).
23. Jaiswal, N. Patel, D.C. Kothari, A. Miotello, Appl. Catal. B: Environ. 126, 47-54 (2012).
24. Venkatachalam, M. Palanichamy, B. Arabindoo, V. Murugesan, J. Molec. Catal. A: Chem. 266, 158-165 (2007).
25. S. Meshesha, R.C. Matangi, S.R. Tirukkovalluri, S Bojja, J. Asian Ceram. Soc. 5, 136–143 (2017).
26. Sharotri, D. Sharma, D. Sud, J. Mater. Res. and Tech. 8, 3995-4009 (2019).
27. D. Chekuri, S.R. Tirukkovalluri, South Afri. J. Chem. Eng. 24, 183-195 (2017).
28. R. Deng, Y. Gao, X.H. Xia, R. S. Chen, L. Wan, G. Shoa, J. Physics: Conf. Series. 152, 12073 (2009).
29. Lenik, D. Verhovek, MTAEC9, 52(4), 411-416 (2018).
30. A. Behnajady, B. Alizade, N. Modirshahla, Photochem. Photobiol. 87, 1308–1314 (2011).
31. M. Mohamed, M.M. Al-Esaimi, J. Mol. Catal. A: Chem. 255, 53-61 (2006).
32. Z. Tang, H. An, Chemosphere. 31, 4157-4170 (1995).
33. Venkatachalam, M. Palanichamy, V. Murugesan, J. Mol. Catal. A; Chem. 273, 177–185 (2007).
34. Subramani, K. Byrappa, S. Ananda, K. Lokanatha rai, C. Ranganathaiah, M. Yoshimura, Bull. Mater. Sci. 30, 37–41 (2007).

Tables

Table.1

Name assigned to different TiO_2 nanocatalyst samples

S.No.	Weight percentages of dopants (Wt%)	Gemini Surfactant Wt%	Name given to the Sample
1.	0.25 Mn 0.75 Mg	-	MMT1
2.	0.75 Mn 0.25 Mg	-	MMT2
3.	0.50 Mn 0.50 Mg	-	MMT3
4.	1.00 Mn 0.25 Mg	-	MMT4
5.	0.25 Mn 1.00 Mg	-	MMT5
6.	0.25 Mn 1.00 Mg	5	MMT5-GS1
7.	0.25 Mn 1.00 Mg	10	MMT5-GS2
8.	0.25 Mn 1.00 Mg	15	MMT5-GS3
9.	NIL	-	Undoped TiO_2

Table.2. Crystallite size, band gap energy and BET surface area of undoped TiO_2 and all bimetal doped and surfactant assisted TiO_2 catalysts calcined at 450 ^oC.

S.No	Nanomaterials	Crystallite size (nm)	Band gap energy (eV)	BET surface analysis		
				Surface area (m^2/g)	Pore volume (cm^3/g)	Pore size (nm)
1	Undoped TiO_2	18.30	3.20	64.09	0.22	10
2	MMT1	12.87	2.97	84.73	0.23	7.3
3	MMT2	12.05	2.83	83.66	0.22	7.2
4	MMT3	11.37	2.79	94.85	0.23	9.3
5	MMT4	11.74	2.75	91.36	0.24	8.1
6	MMT5	10.86	2.68	112.03	0.24	7.0
7	MMT5-GS1	10.22	2.76	140.61	0.24	7.3
8	MMT5-GS2	7.21	2.66	230.20	0.25	6.4
9	MMT5-GS3	8.33	2.83	160.14	0.22	8.3

Table.3. Comparative study of Mn^{2+}, Mg^{2+} single doped and Mn^{2+}/Mg^{2+} bimetal doped TiO_2 nanocatalysts.

TiO_2 Catalyst	Band gap Energy (eV)	Surface Area (m^2/g)	Crystallite Size (nm)	Reference No.
Mn-TiO_2	2.98	93	21.8	[29]
Mg-TiO_2	2.92	48.5	20	[30]
Undoped TiO_2	3.2	64.09	18.3	Present work
MMT5	2.68	112.03	10.86	Present work
MMT5-GS2	2.66	230.20	7.21	Present work

Figures

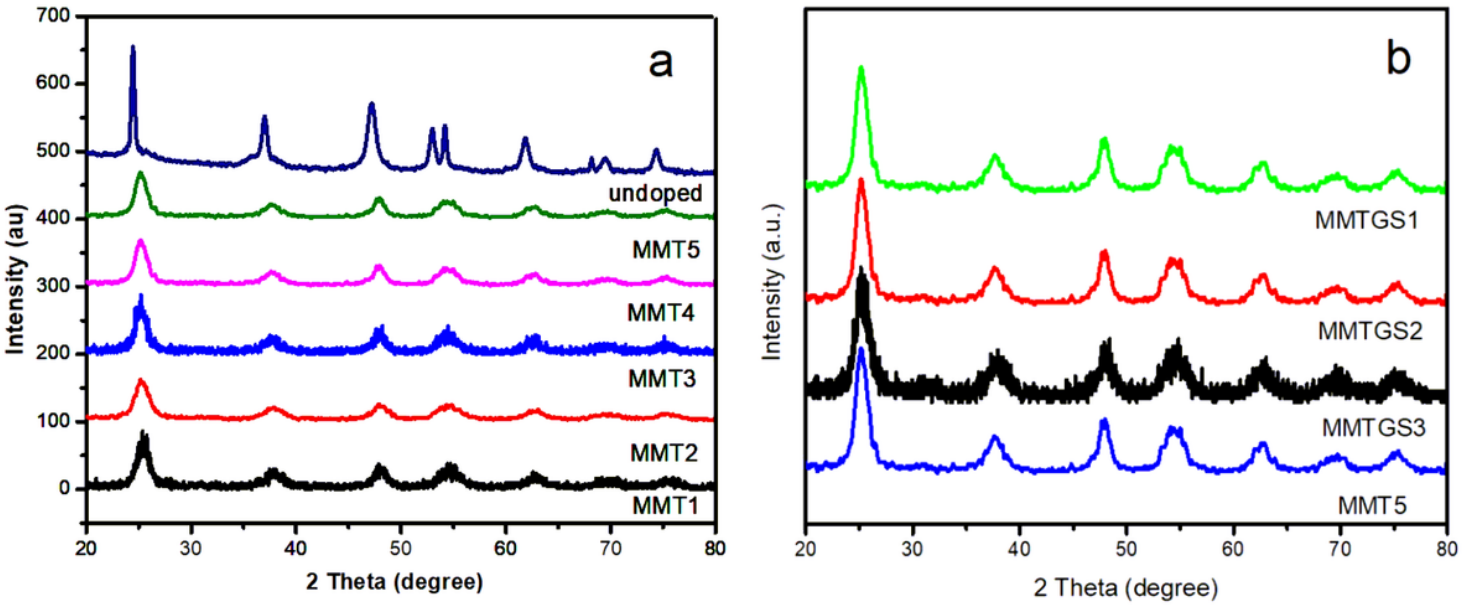

Figure 1

(a) XRD patterns of undoped TiO2 and Mn2+/Mg2+ bimetal doped TiO2 (MMT1-MMT5) catalysts. (b) MMT5 and Surfactant assisted catalysts (MMT5-GS1- MMT5-GS3).

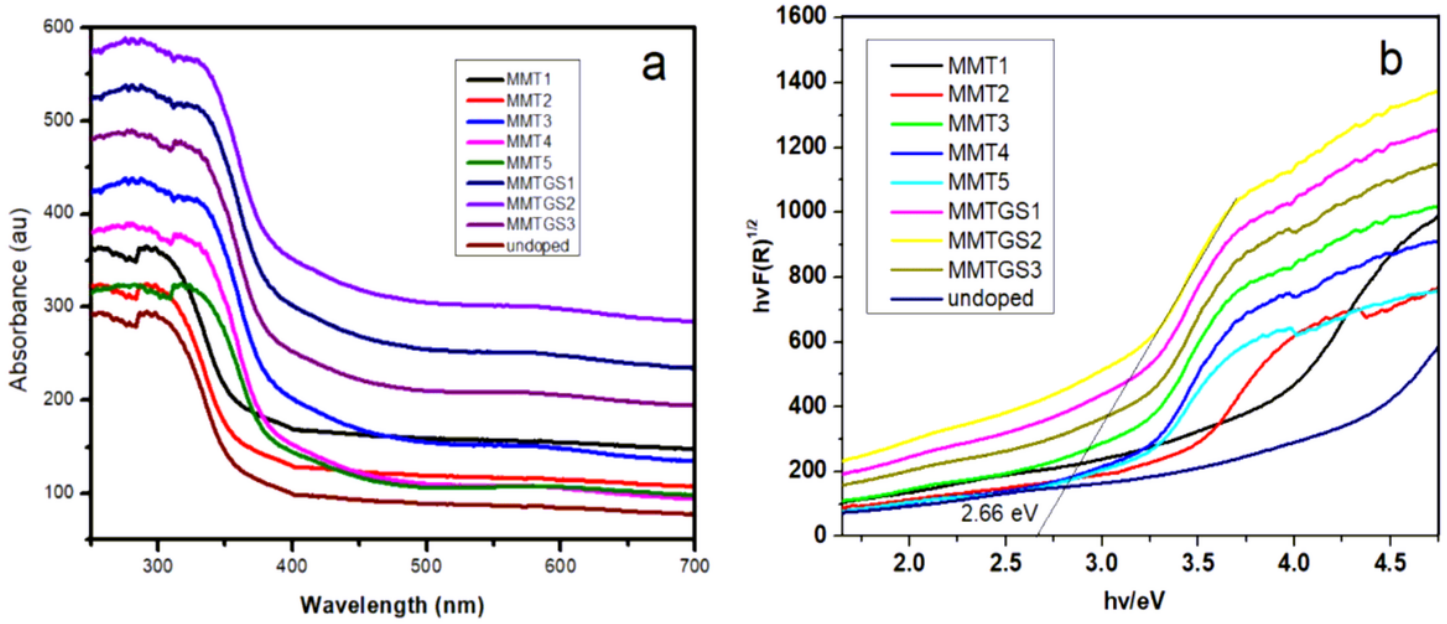

Figure 2

(a) UV-Vis DRS and (b) Kubelka-Munk formalism spectra of undoped TiO2, MMT and MMT5-GS catalysts.

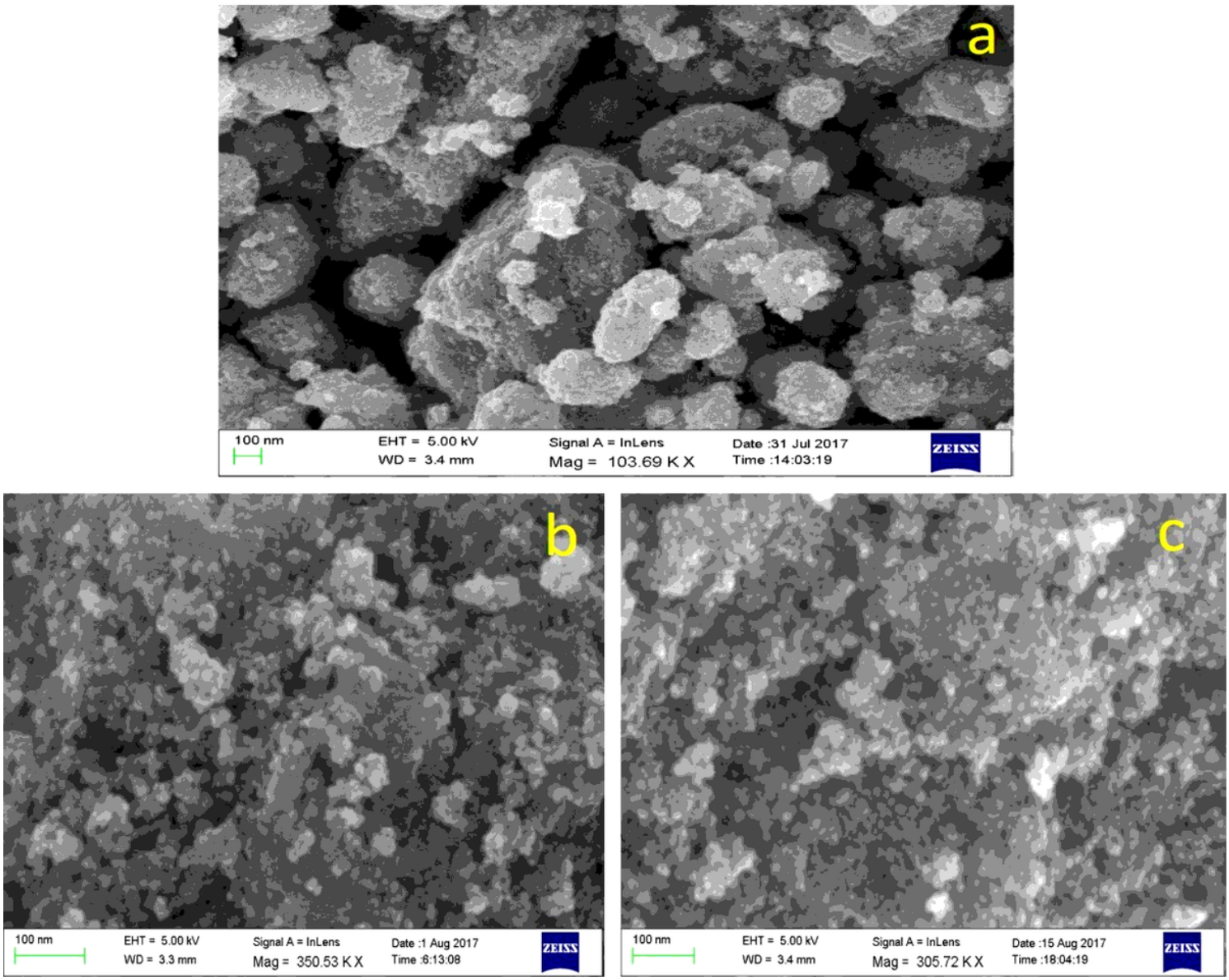

Figure 3

SEM micrographs of (a) Undoped TiO2, (b) MMT5 and (c) MMT5-GS2

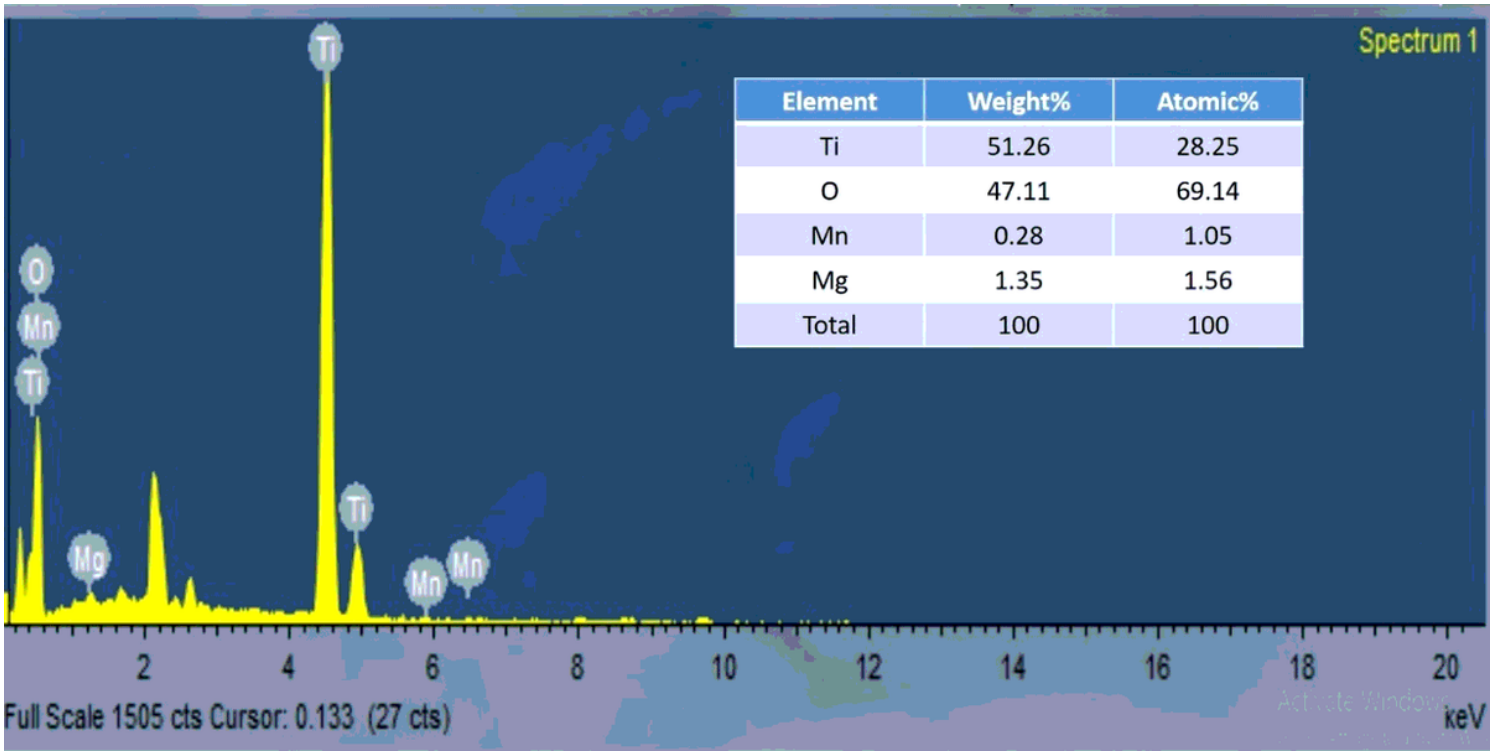

Figure 4

EDX spectrum of 0.25 wt% Mn2+& 1.00 wt% Mg2+ bimetal doped TiO2 in presence of 10 wt% of surfactant (MMT5-GS2) after calcination.

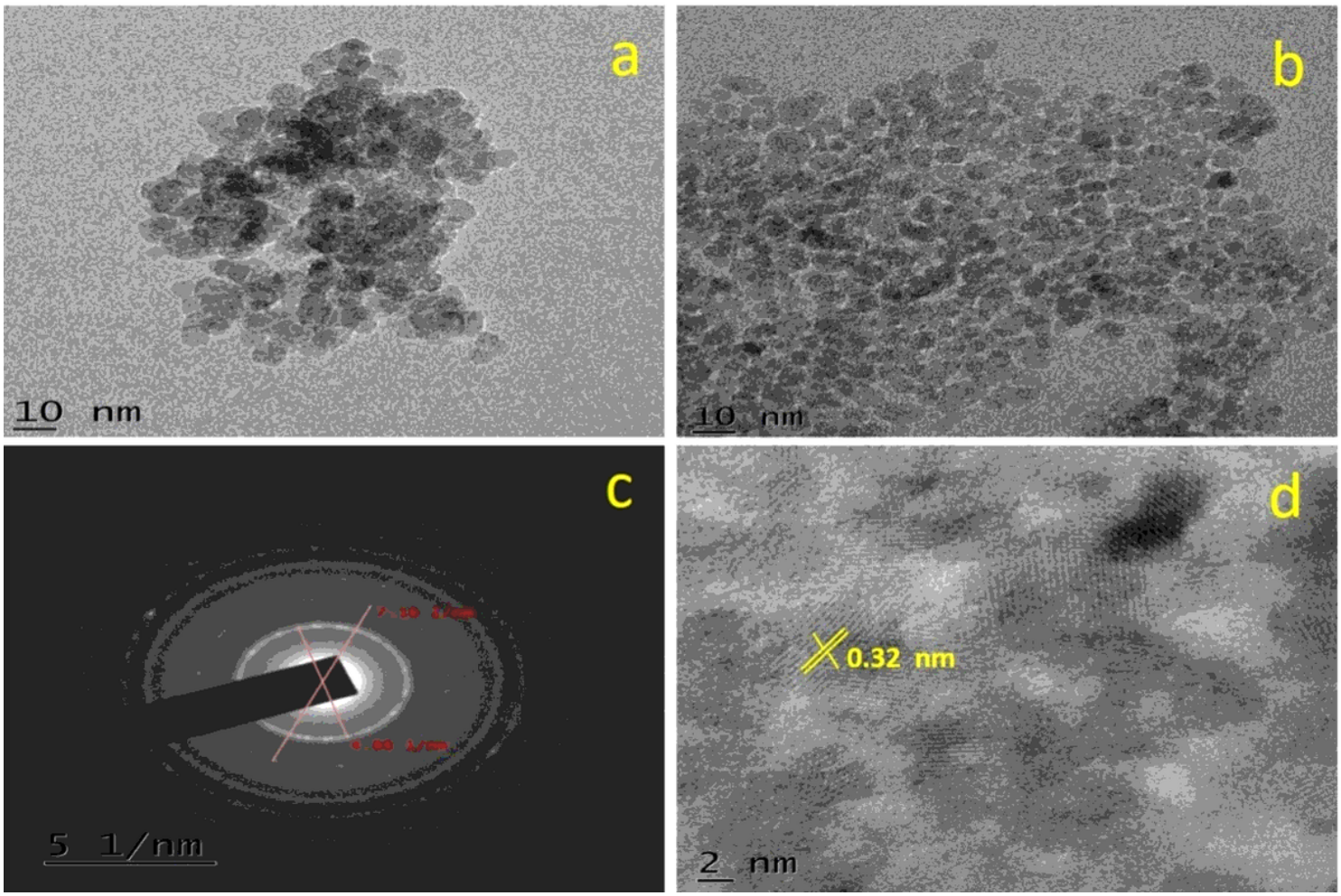

Figure 5

TEM image of (a) MMT5, (b) MMT5-GS2, (c) Selected area electron diffraction (SEAD) and (d) HRTEM Image of MMT5-GS2.

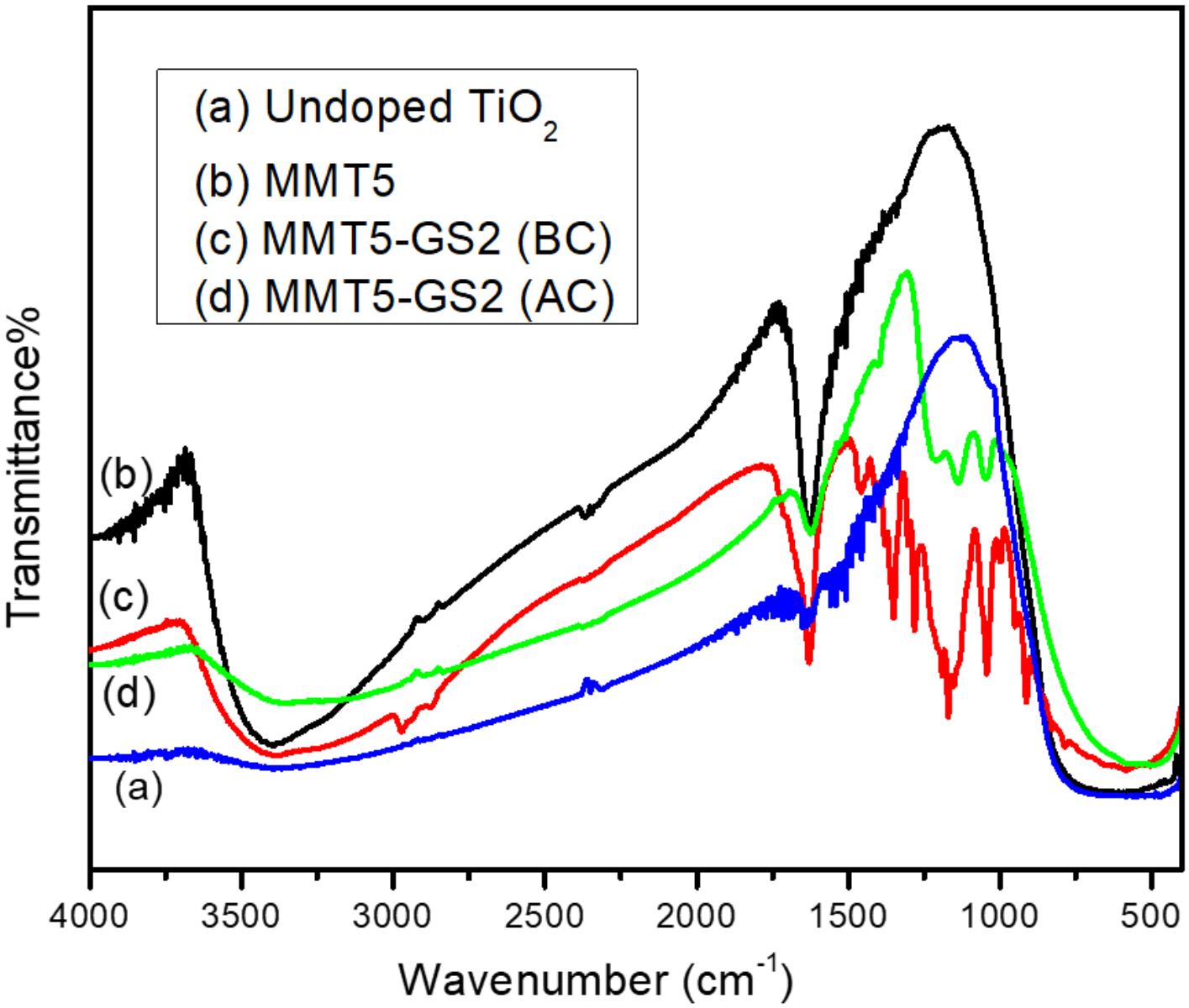

Figure 6

(a) FT-IR spectra of undoped TiO2, (b) MMT5, (c) MMT5-GS2 (BC), (d) FT-IR spectra of MMT5-GS2 (AC).

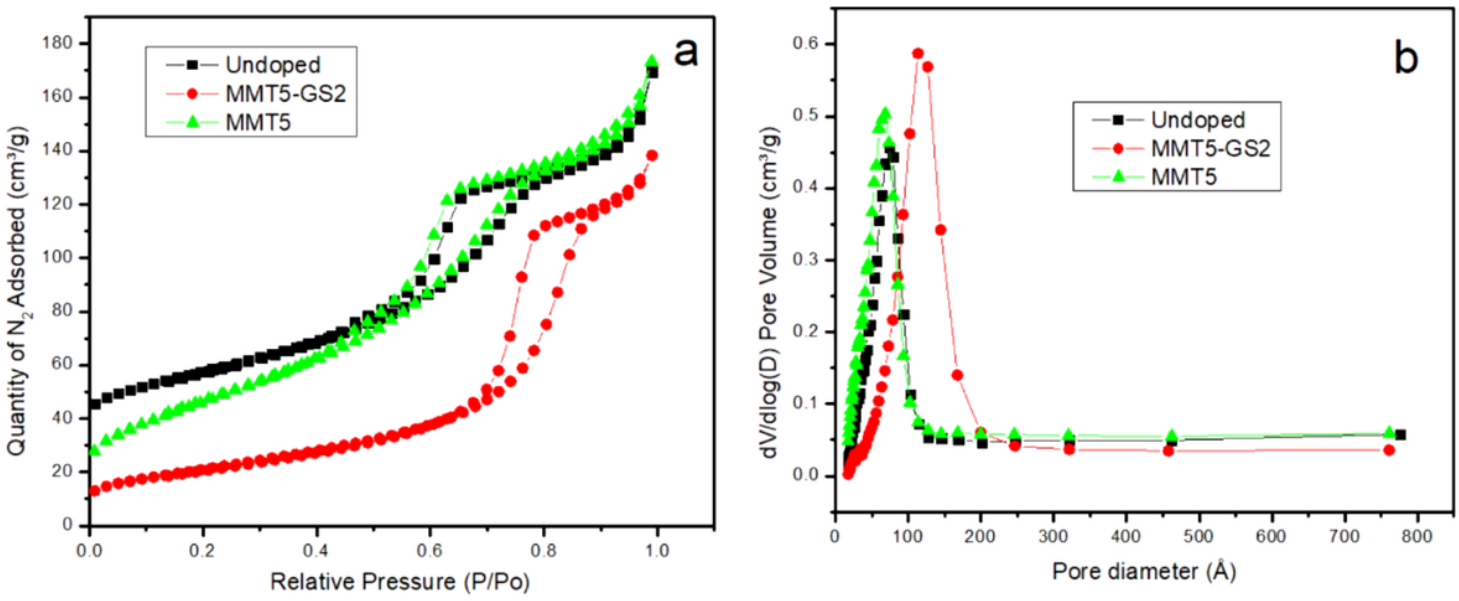

Figure 7

(a) N2 adsorption-desorption isotherm plot and (b) pore size distribution of undoped TiO2, MMT5 and MMT5-GS2.

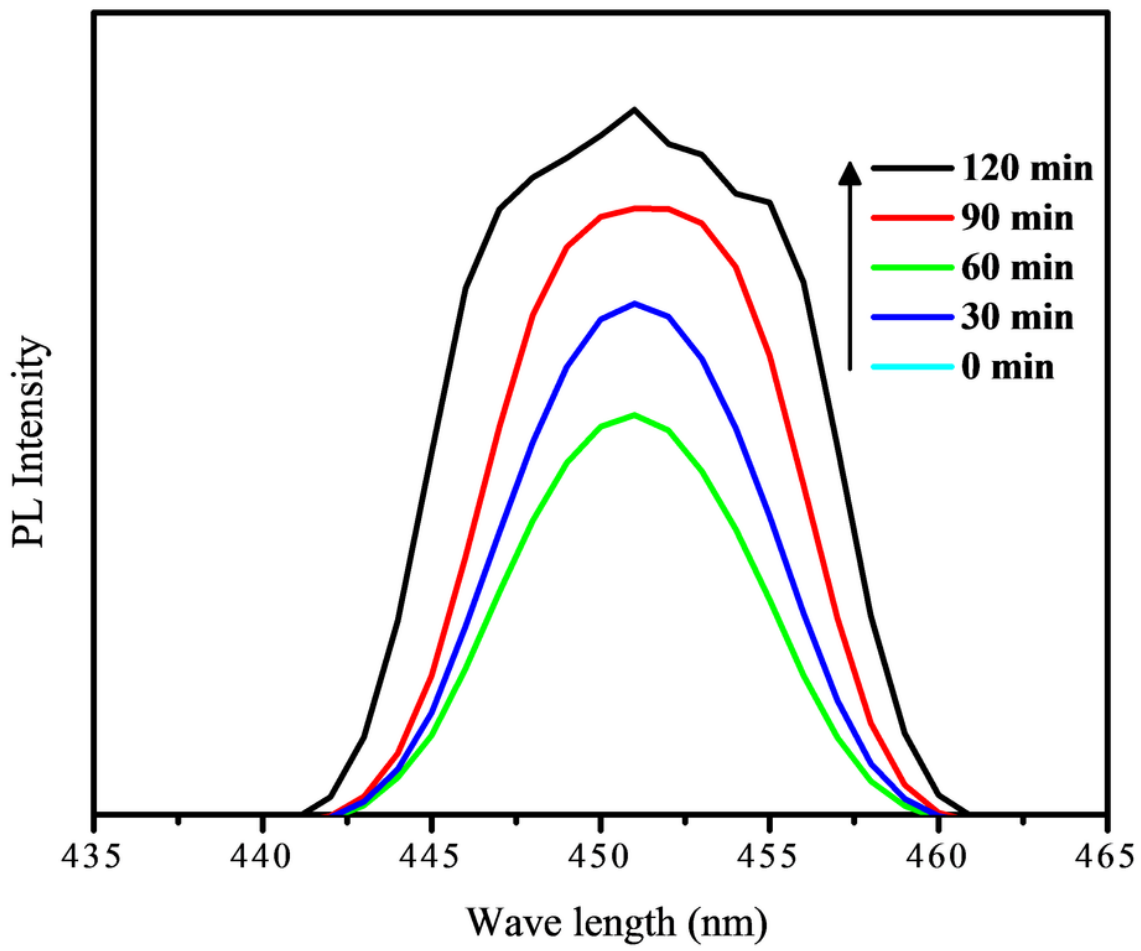

Figure 8

Photoluminescence spectra of MMT5-GS2

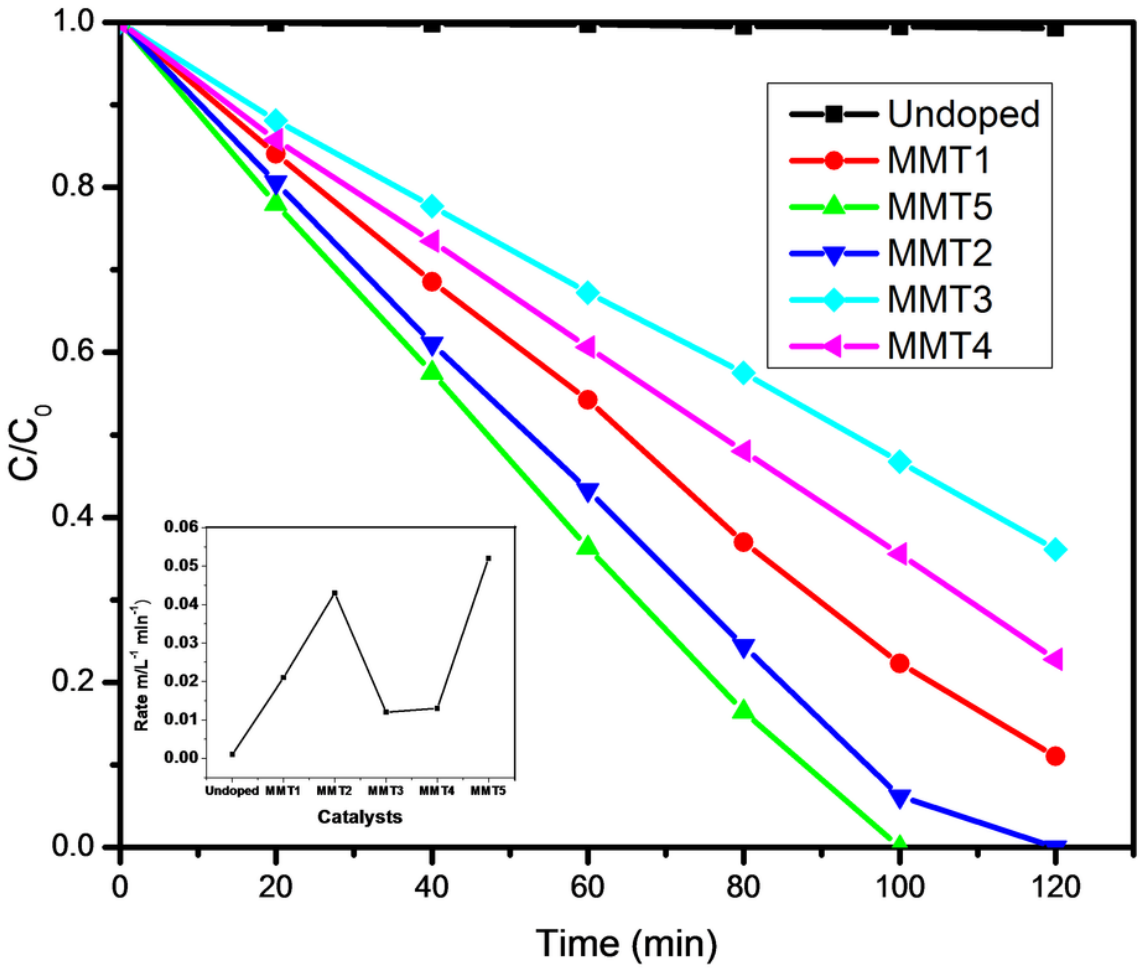

Figure 9

Effect of dopant concentration of bimetal doped TiO2 on photocatalytic degradation of MR dye. Here, catalyst dosage 0.05 g, pH-4 and [MR]= 10 mg/L

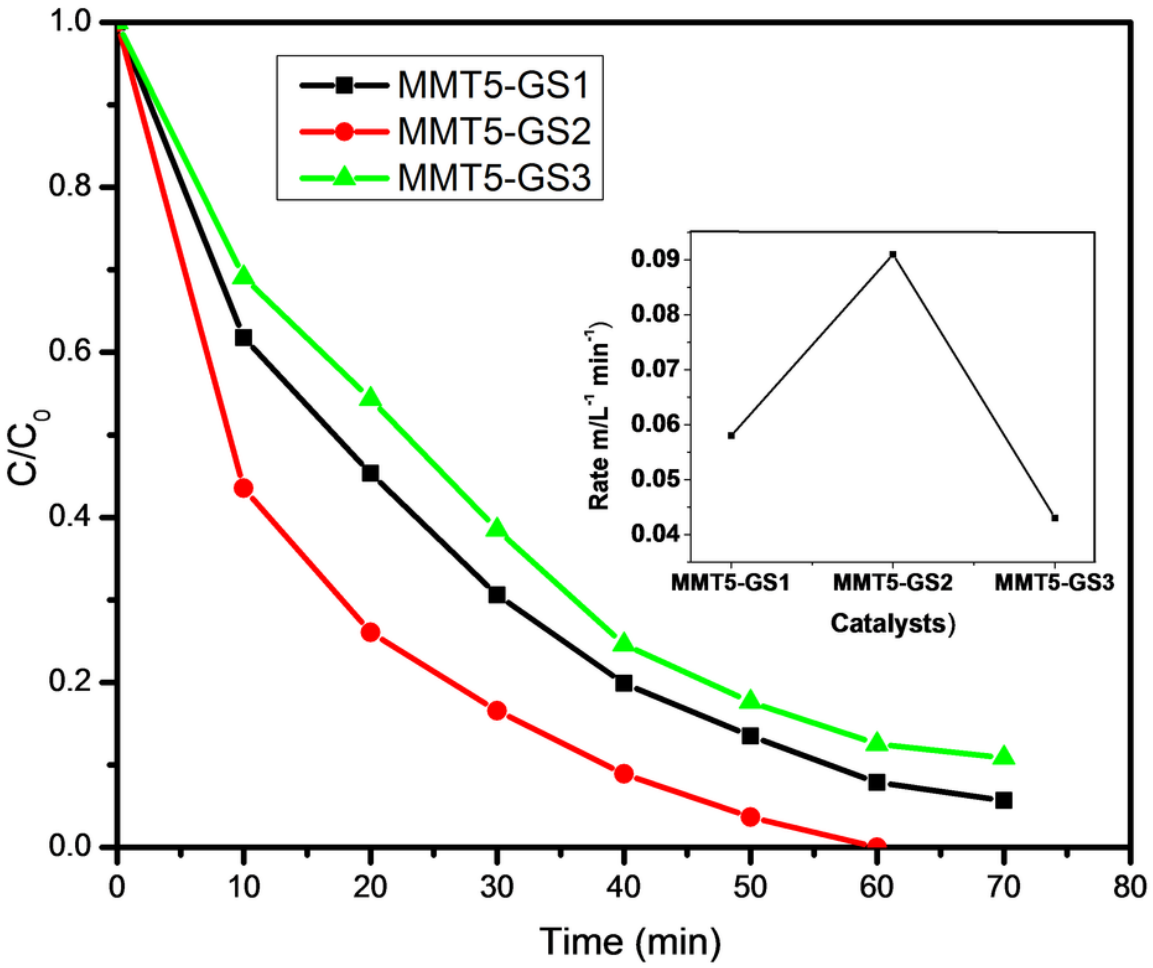

Figure 10

Effect of GS concentration on the photocatalytic activity of MMT5 on the degradation of MR. Here catalyst dosage is 0.05 g, pH 4 and [MR] = 10 mgL-1.

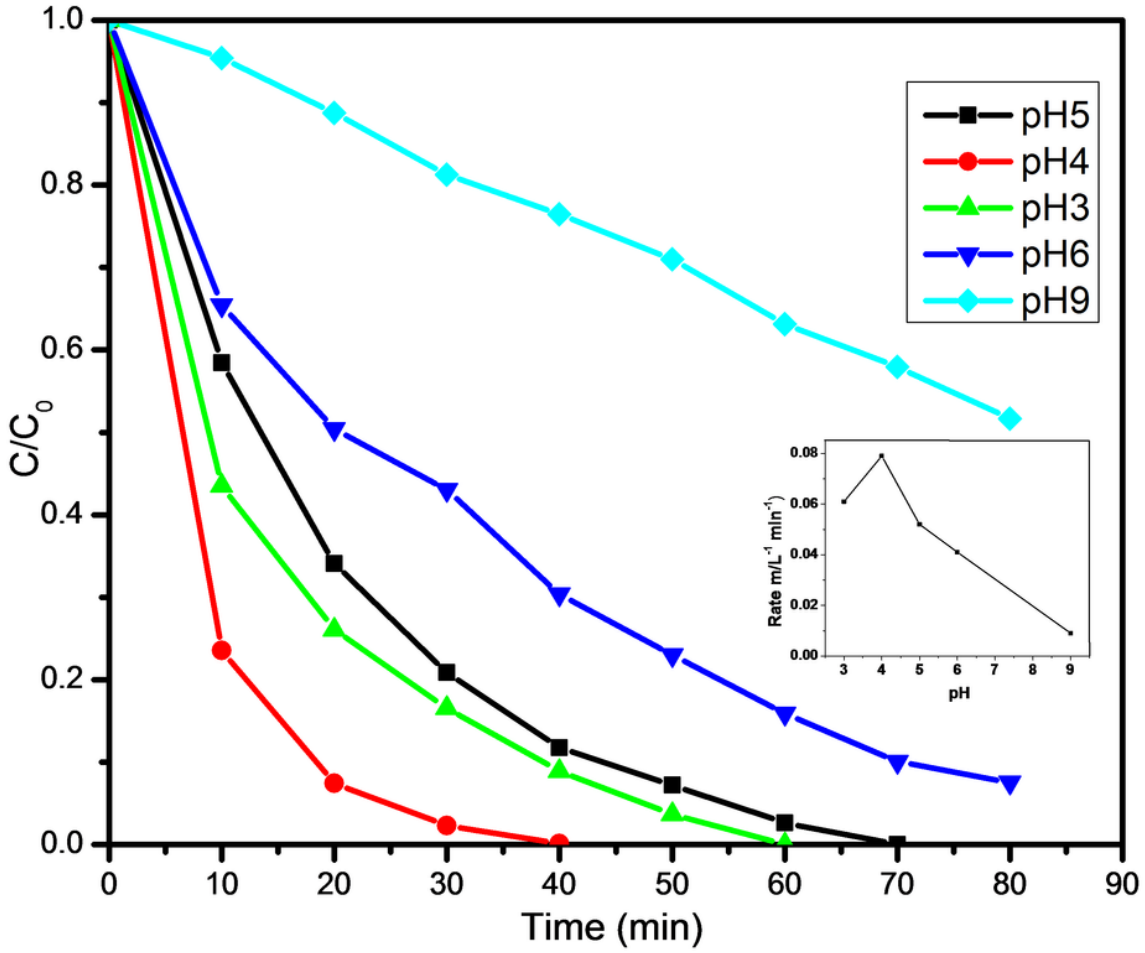

Figure 11

The effect of pH on the rate of degradation of MR dye by MMT5-GS2. Here, catalyst dosage 0.1 g and [MR]=10 mg/L.

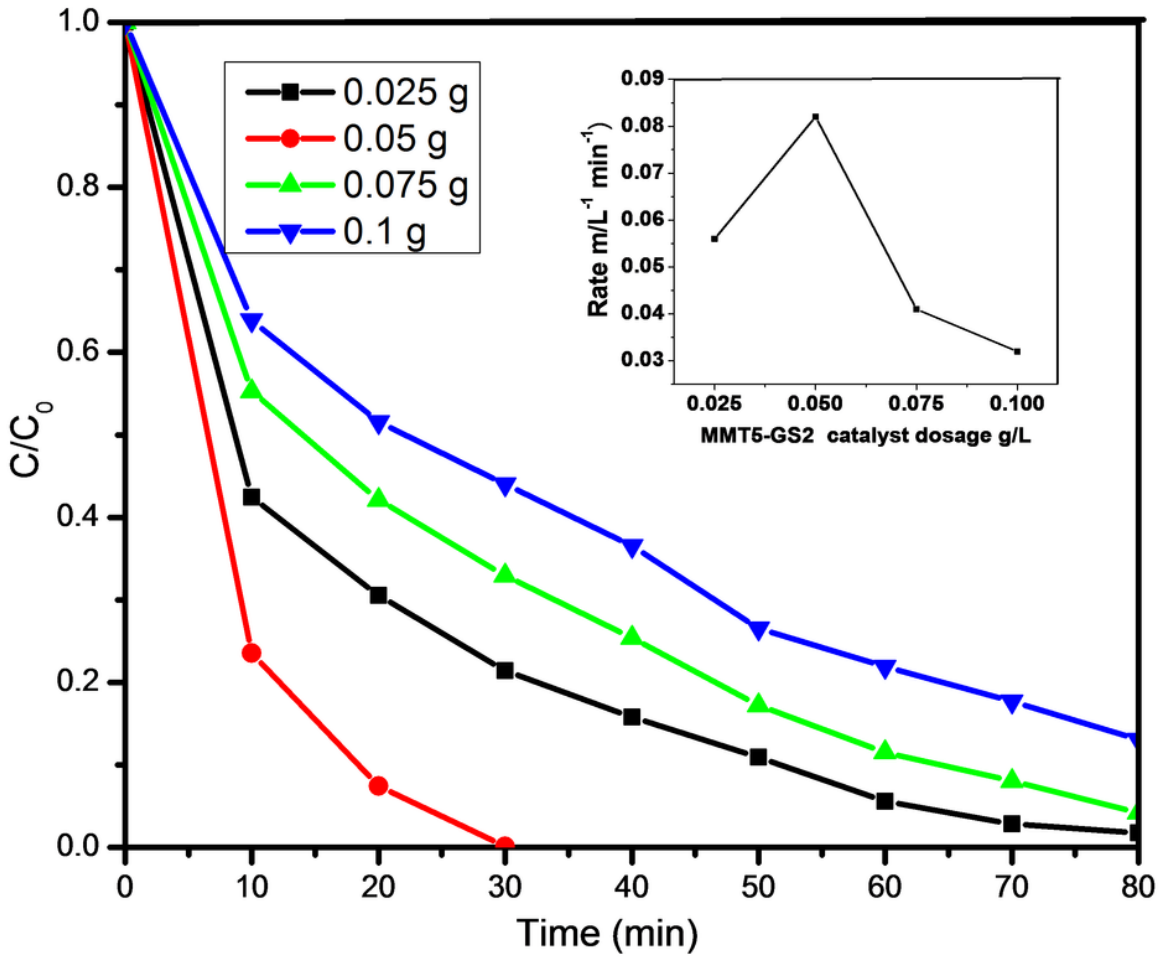

Figure 12

Effect of catalyst dosage on the degradation of MR by MMT5-GS2, here pH 4 and [MR] =10 mg/L.

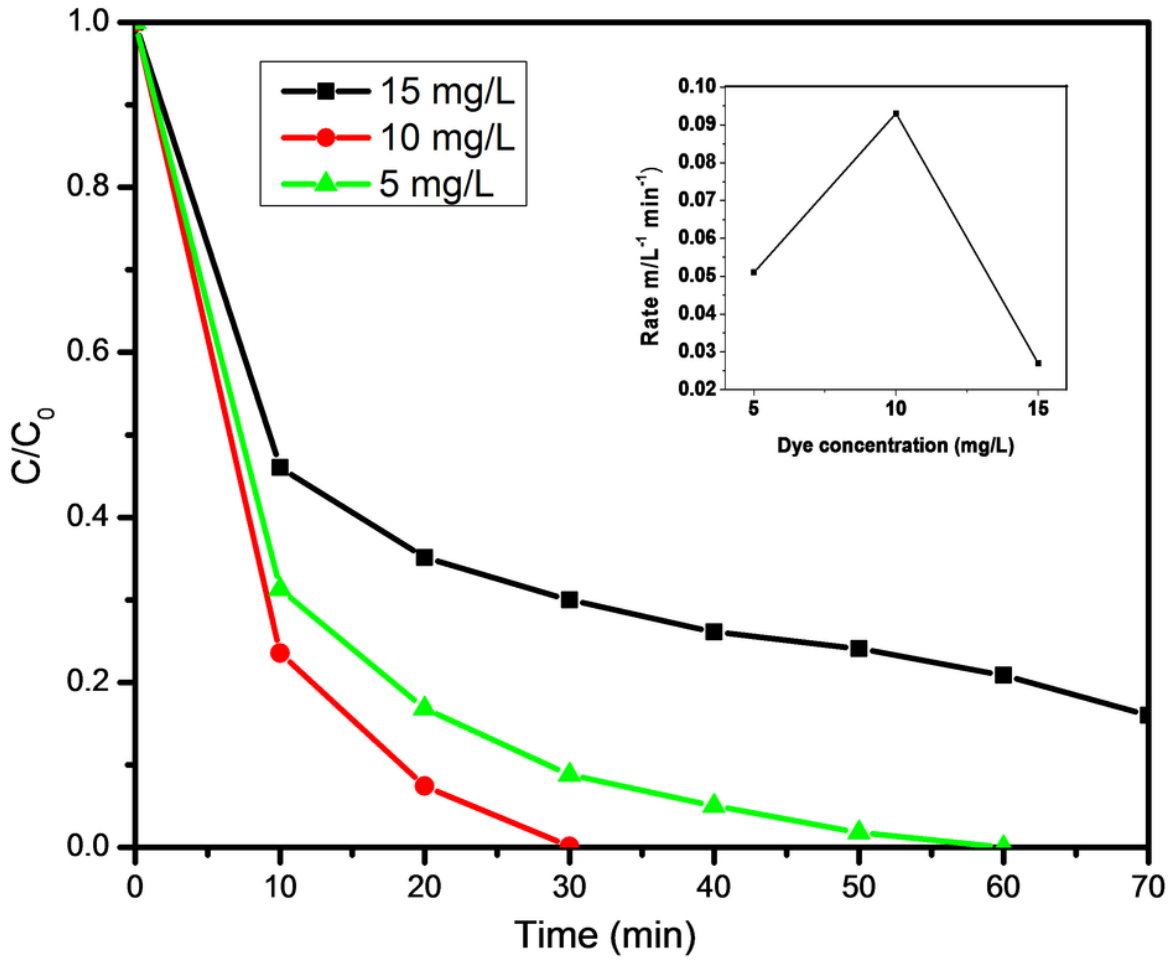

Figure 13

Effect of initial concentration of the dye on the rate of degradation of MR dye by MMT5-GS2, here pH=4 and catalyst dosage 0.05 g.

Supplementary Files

This is a list of supplementary files associated with this preprint. Click to download.

- Supplementaryfile.docx